

Supplementary material to "Slab Break-offs in the Alpine Subduction Zone "

Contents of this file

1. Table S1
2. Figures S1 to S10

5 **Introduction** The supplementary material gives a side-by-side comparison of the nine tomographic models discussed in the main article in Figures S1–S10, and a summary of the findings on the eastern Alpine slab geometry and amount of shortening in Table S1. Figure S1 shows the models in map view at a depth of 150 km, Figures S2–S10 show the models along different cross-sections. Not all models cover the entire region. If a model has no resolution at all along a certain section, it is not shown.
10 The color map is the same for all plotted models, however, the color scale is different in order to have the best comparability of the slab geometries.

Table S1. Main observations concerning the subduction in the eastern Alps.

Depth of slab tip (variable along latitude)	250 km (Lippitsch et al., 2003) > 400 km (Koulakov et al., 2009) > 400 km (Dando et al., 2011) > 400 km (Mitterbauer et al., 2011) > 400 km (Zhao et al., 2016) > 400 km (Hua et al., 2017)
Slab dip	All body-wave tomographic models show a vertical to subvertical, slightly northward dipping slab between 12° and 14° longitude, if the entire slab is taken into account (Lippitsch et al., 2003; Koulakov et al., 2009; Dando et al., 2011; Mitterbauer et al., 2011; Zhao et al., 2016; Hua et al., 2017).
E-W slab continuity	All models show a gap or discontinuity (northward step) between central and eastern Alpine anomalies (Lippitsch et al., 2003; Koulakov et al., 2009; Mitterbauer et al., 2011; Zhao et al., 2016; Hua et al., 2017).
Vertical slab continuity	Lippitsch et al. (2003) show a slab that is continuous from the lithosphere down to 250 km depth. Other authors show a rather continuous slab down to the mantle transition zones (Koulakov et al., 2009; Dando et al., 2011; Mitterbauer et al., 2011; Zhao et al., 2016). Anomaly variations in vertical direction are not interpreted by the authors. The images by Hua et al. (2017) show a significantly weakened anomaly in the upper 200 km. All models that cover areas east of 14°E indicate that the slab anomaly weakens and then disappears in the upper 250 km (Koulakov et al., 2009; Dando et al., 2011; Mitterbauer et al., 2011; Zhao et al., 2016; Hua et al., 2017).
N-S shortening	Total of 190 km, mostly in the southern Alps (Ustaszewski et al., 2008) minimum 55 – 75 km in the southern Alps (Brückl, 2011) minimum 50 km in the southern Alps (Schönböck, 1999; Nussbaum, 2000)
Moho offset	An offset suggesting that Europe is the lower plate is only imaged along the TRANSALP cross-section in the work of Kummerow et al. (2004). This may be due to indentation of Adria at mid-crustal levels. More recent results suggest rather that the Moho structure is ambiguous in this area (e.g., Spada et al., 2013). Hetényi et al. (2018) confirm the ambiguity of Moho structure in this area but find indications of deeper Adriatic Moho.

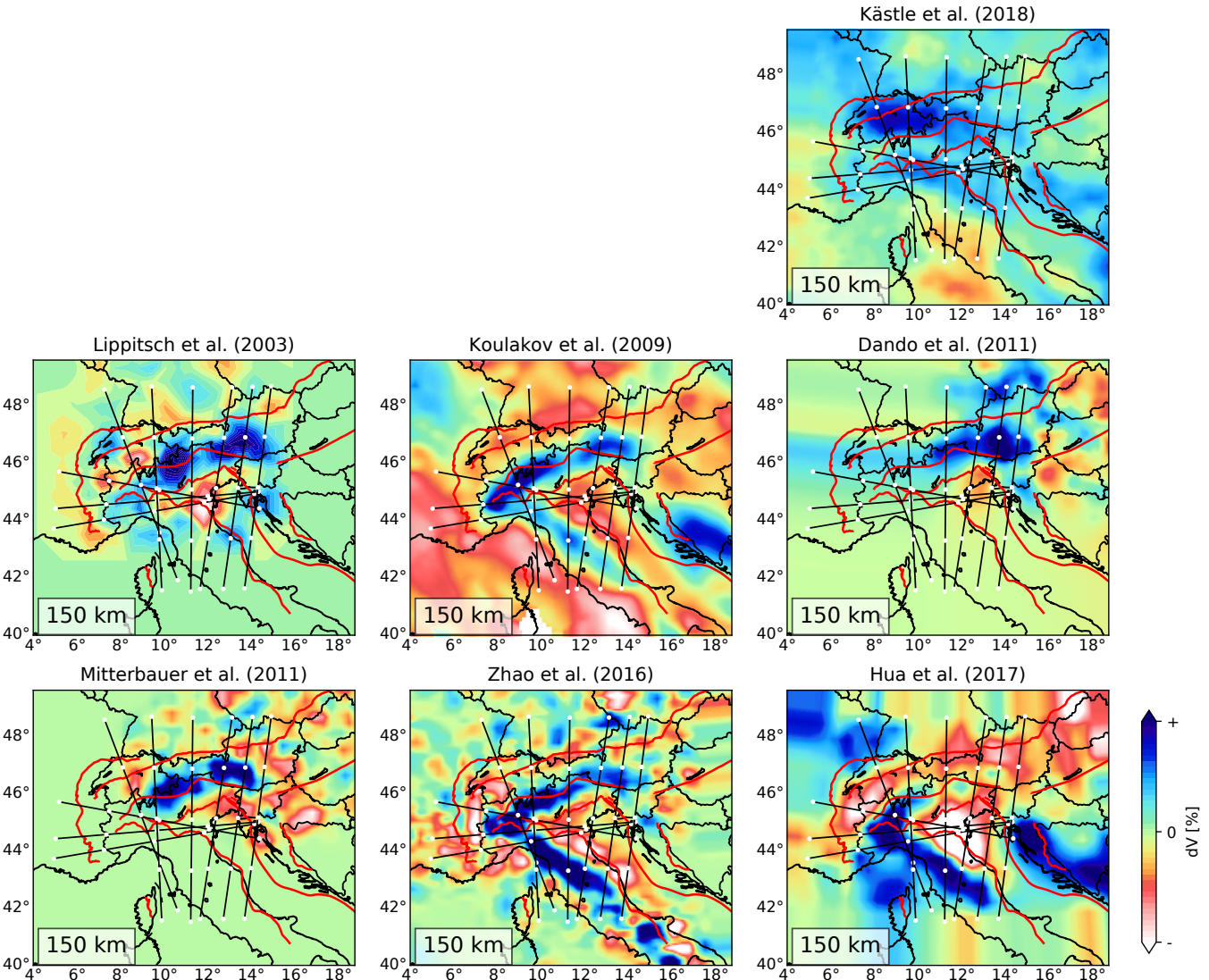


Figure S1. Map comparison of different tomographic models at 150 km depth. The colors show either shear-velocity deviations (Kästle et al., 2018) or compressional-velocity deviations (other models) of PREM (Dziewonski and Anderson, 1981). The color scale is normalized to $\pm 5\%$ for Lippitsch et al. (2003), $\pm 3.5\%$ for Kästle et al. (2018), $\pm 3\%$ for Koulakov et al. (2009); Zhao et al. (2016) and $\pm 2\%$ for the other models. In most models, only central parts of the shown region are well resolved. Faults and tectonic limits (red lines) simplified from Schmid et al. (2004, 2008); Handy et al. (2010).

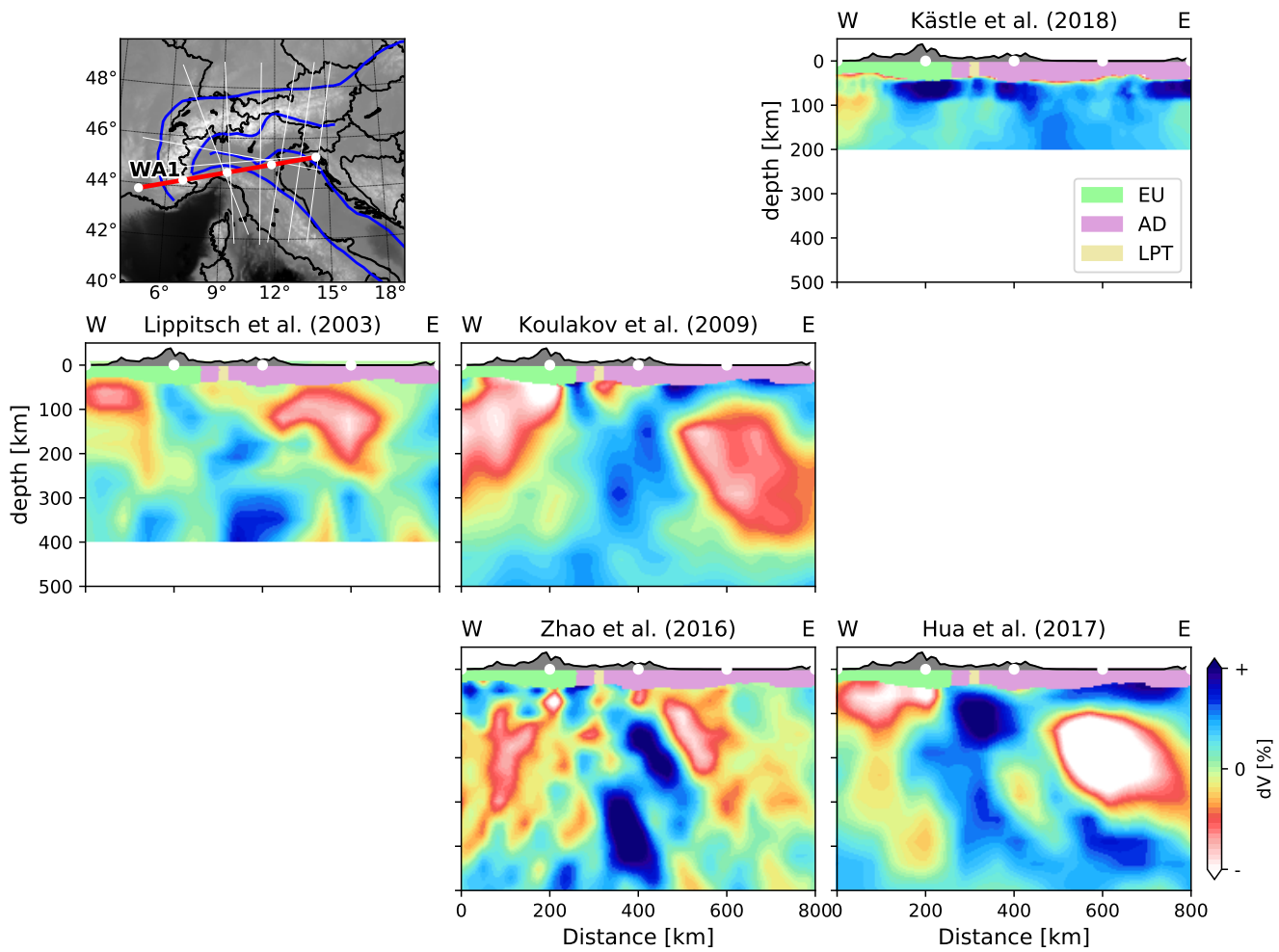


Figure S2. Cross-section comparison of different tomographic models. Models that do not cover the crossed region are not shown. The colors show either shear-velocity deviations (Kästle et al., 2018) or compressional-velocity deviations (other models) of PREM (Dziewonski and Anderson, 1981). The color scale is normalized to $\pm 5\%$ for Lippitsch et al. (2003), $\pm 3.5\%$ for Kästle et al. (2018), $\pm 3\%$ for Koulakov et al. (2009); Zhao et al. (2016) and $\pm 2\%$ for the other models. Moho boundaries from Spada et al. (2013). EU: Europe, AD: Adria, LPT: Liguro-Provençal and Tyrrhenian basins. Faults and tectonic limits (blue lines in the map) simplified from Schmid et al. (2004, 2008); Handy et al. (2010).

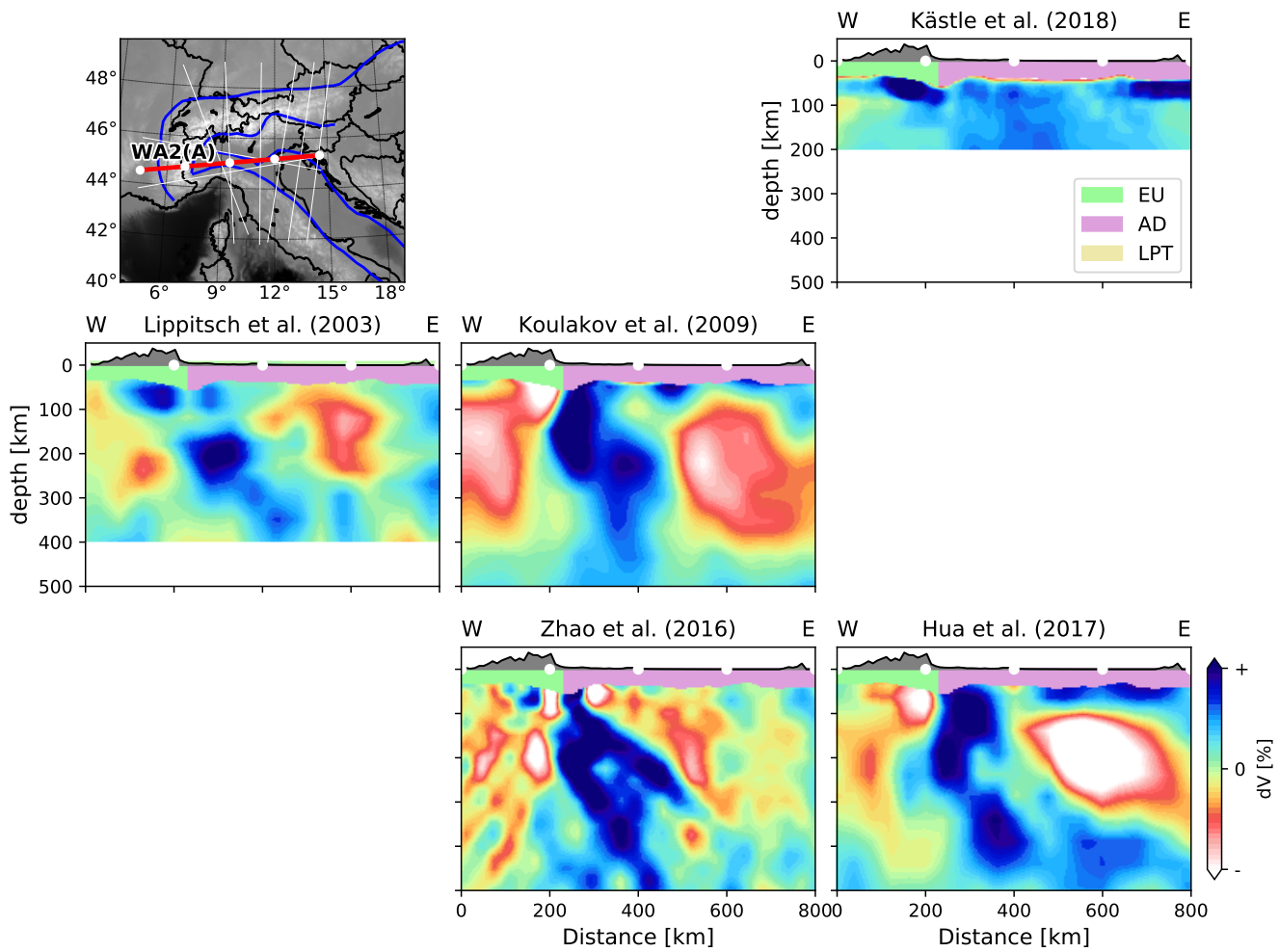


Figure S3. Cross-section comparison of different tomographic models. Models that do not cover the crossed region are not shown. The colors show either shear-velocity deviations (Kästle et al., 2018) or compressional-velocity deviations (other models) of PREM (Dziewonski and Anderson, 1981). The color scale is normalized to $\pm 5\%$ for Lippitsch et al. (2003), $\pm 3.5\%$ for Kästle et al. (2018), $\pm 3\%$ for Koulakov et al. (2009); Zhao et al. (2016) and $\pm 2\%$ for the other models. Moho boundaries from Spada et al. (2013). EU: Europe, AD: Adria, LPT: Liguro-Provençal and Tyrrhenian basins. Faults and tectonic limits (blue lines in the map) simplified from Schmid et al. (2004, 2008); Handy et al. (2010).

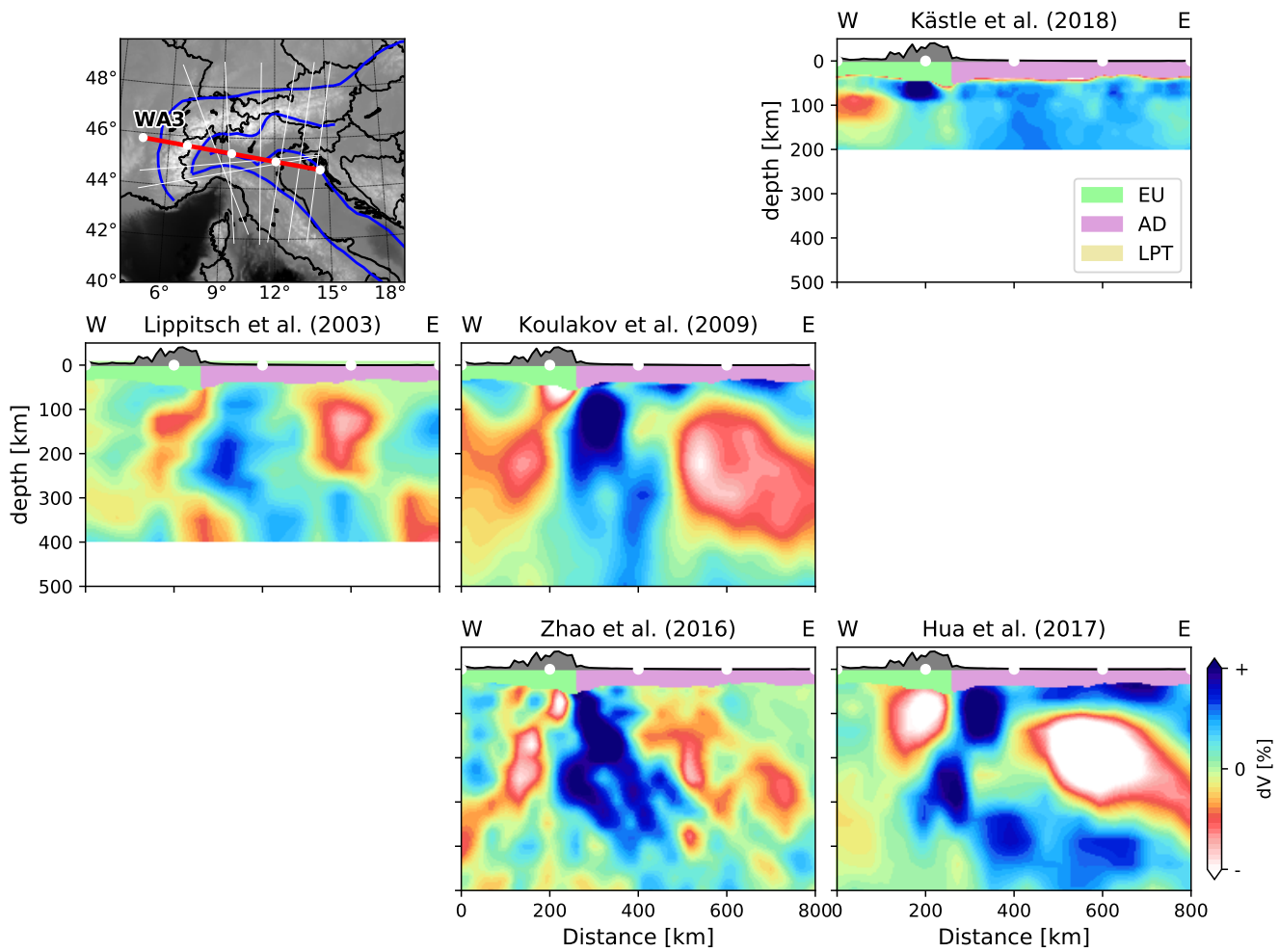


Figure S4. Cross-section comparison of different tomographic models. Models that do not cover the crossed region are not shown. The colors show either shear-velocity deviations (Kästle et al., 2018) or compressional-velocity deviations (other models) of PREM (Dziewonski and Anderson, 1981). The color scale is normalized to $\pm 5\%$ for Lippitsch et al. (2003), $\pm 3.5\%$ for Kästle et al. (2018), $\pm 3\%$ for Koulakov et al. (2009); Zhao et al. (2016) and $\pm 2\%$ for the other models. Moho boundaries from Spada et al. (2013). EU: Europe, AD: Adria, LPT: Liguro-Provençal and Tyrrhenian basins. Faults and tectonic limits (blue lines in the map) simplified from Schmid et al. (2004, 2008); Handy et al. (2010).

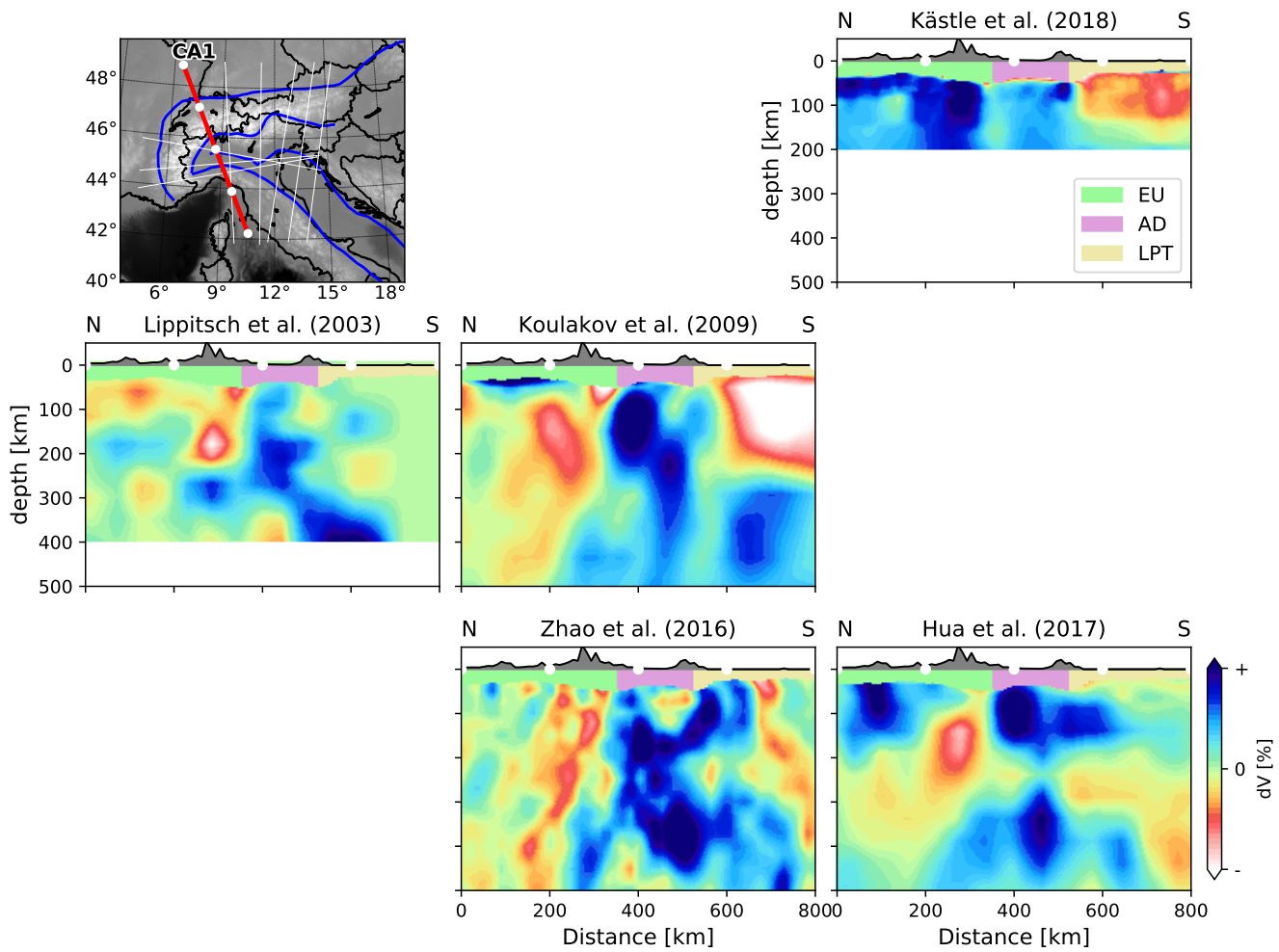


Figure S5. Cross-section comparison of different tomographic models. Models that do not cover the crossed region are not shown. The colors show either shear-velocity deviations (Kästle et al., 2018) or compressional-velocity deviations (other models) of PREM (Dziewonski and Anderson, 1981). The color scale is normalized to $\pm 5\%$ for Lippitsch et al. (2003), $\pm 3.5\%$ for Kästle et al. (2018), $\pm 3\%$ for Koulakov et al. (2009); Zhao et al. (2016) and $\pm 2\%$ for the other models. Moho boundaries from Spada et al. (2013). EU: Europe, AD: Adria, LPT: Liguro-Provençal and Tyrrhenian basins. Faults and tectonic limits (blue lines in the map) simplified from Schmid et al. (2004, 2008); Handy et al. (2010).

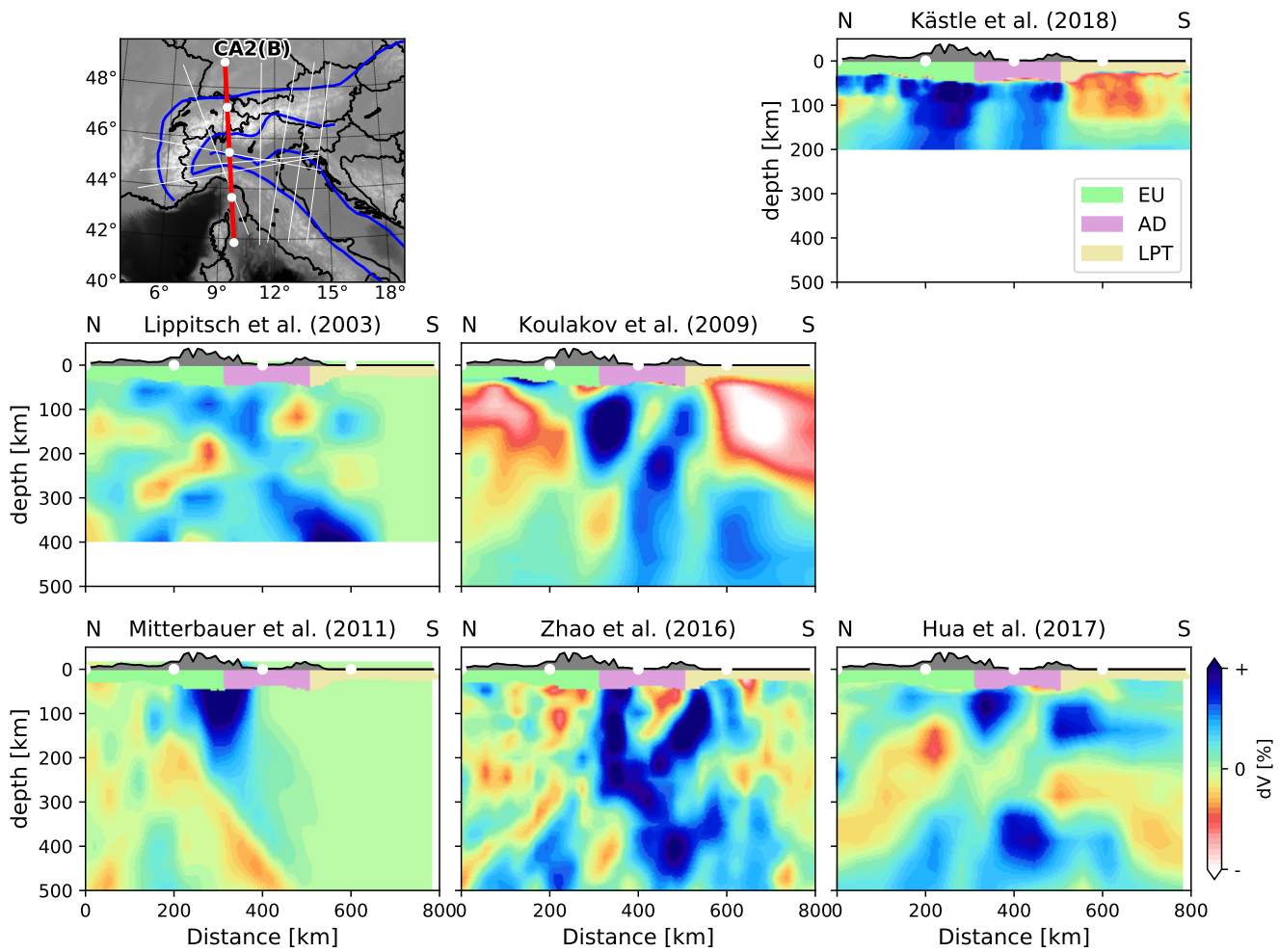


Figure S6. Cross-section comparison of different tomographic models. Models that do not cover the crossed region are not shown. The colors show either shear-velocity deviations (Kästle et al., 2018) or compressional-velocity deviations (other models) of PREM (Dziewonski and Anderson, 1981). The color scale is normalized to $\pm 5\%$ for Lippitsch et al. (2003), $\pm 3.5\%$ for Kästle et al. (2018), $\pm 3\%$ for Koulakov et al. (2009); Zhao et al. (2016) and $\pm 2\%$ for the other models. Moho boundaries from Spada et al. (2013). EU: Europe, AD: Adria, LPT: Liguro-Provençal and Tyrrhenian basins. Faults and tectonic limits (blue lines in the map) simplified from Schmid et al. (2004, 2008); Handy et al. (2010).

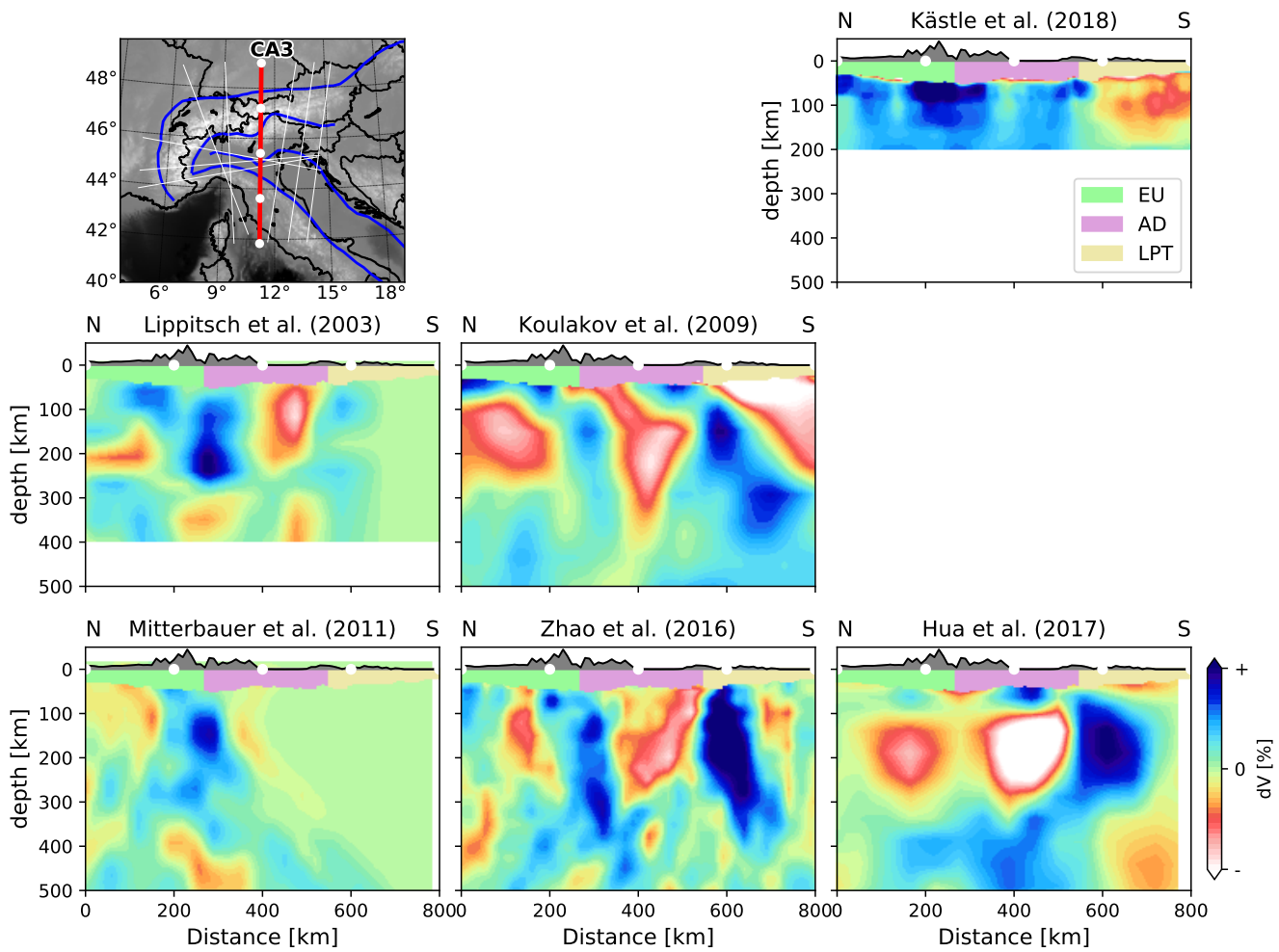


Figure S7. Cross-section comparison of different tomographic models. Models that do not cover the crossed region are not shown. The colors show either shear-velocity deviations (Kästle et al., 2018) or compressional-velocity deviations (other models) of PREM (Dziewonski and Anderson, 1981). The color scale is normalized to $\pm 5\%$ for Lippitsch et al. (2003), $\pm 3.5\%$ for Kästle et al. (2018), $\pm 3\%$ for Koulakov et al. (2009); Zhao et al. (2016) and $\pm 2\%$ for the other models. Moho boundaries from Spada et al. (2013). EU: Europe, AD: Adria, LPT: Liguro-Provençal and Tyrrhenian basins. Faults and tectonic limits (blue lines in the map) simplified from Schmid et al. (2004, 2008); Handy et al. (2010).

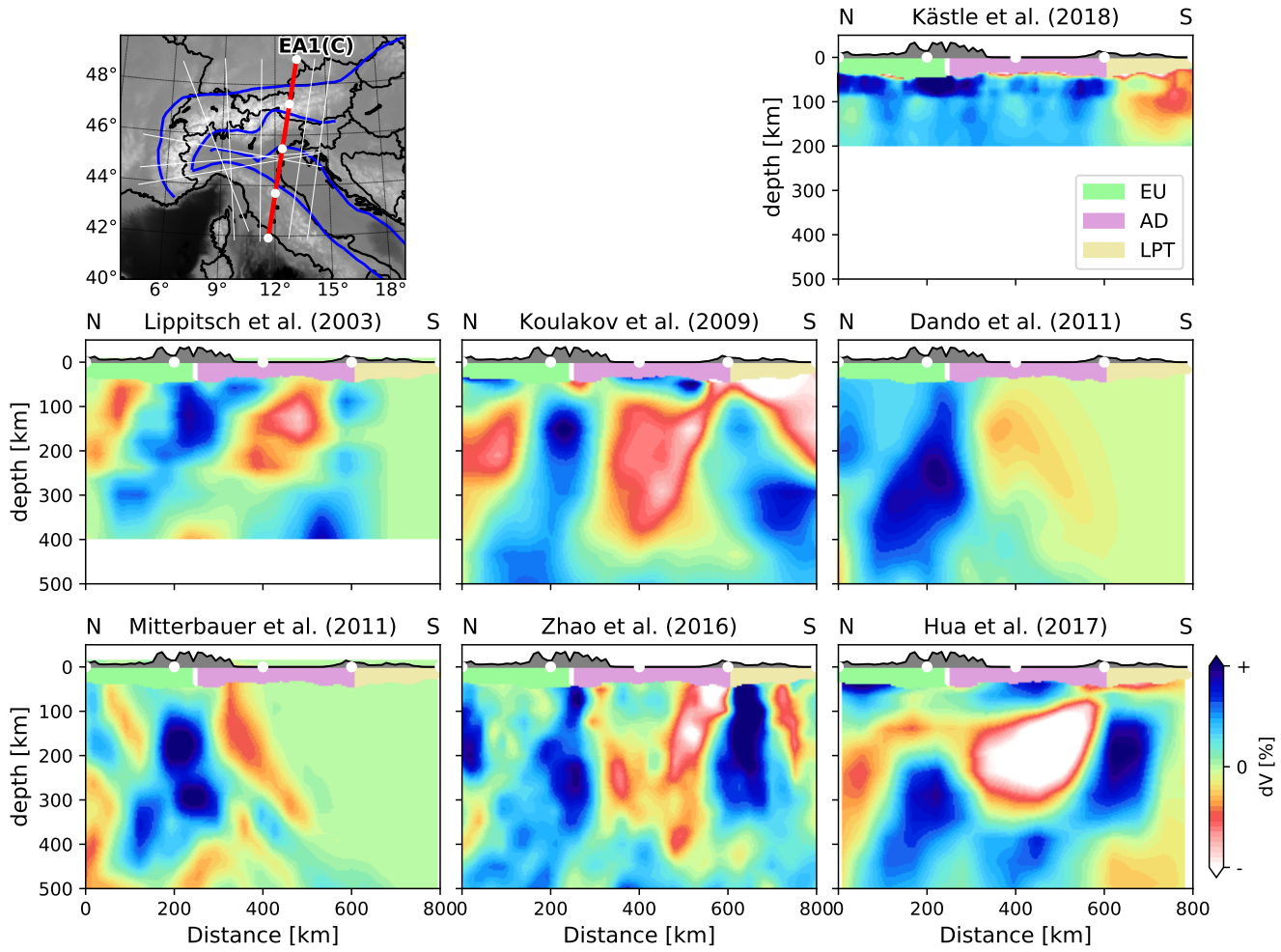


Figure S8. Cross-section comparison of different tomographic models. The colors show either shear-velocity deviations (Kästle et al., 2018) or compressional-velocity deviations (other models) of PREM (Dziewonski and Anderson, 1981). The color scale is normalized to $\pm 5\%$ for Lippitsch et al. (2003), $\pm 3.5\%$ for Kästle et al. (2018), $\pm 3\%$ for Koulakov et al. (2009); Zhao et al. (2016) and $\pm 2\%$ for the other models. Moho boundaries from Spada et al. (2013). EU: Europe, AD: Adria, LPT: Liguro-Provençal and Tyrrhenian basins. Faults and tectonic limits (blue lines in the map) simplified from Schmid et al. (2004, 2008); Handy et al. (2010).

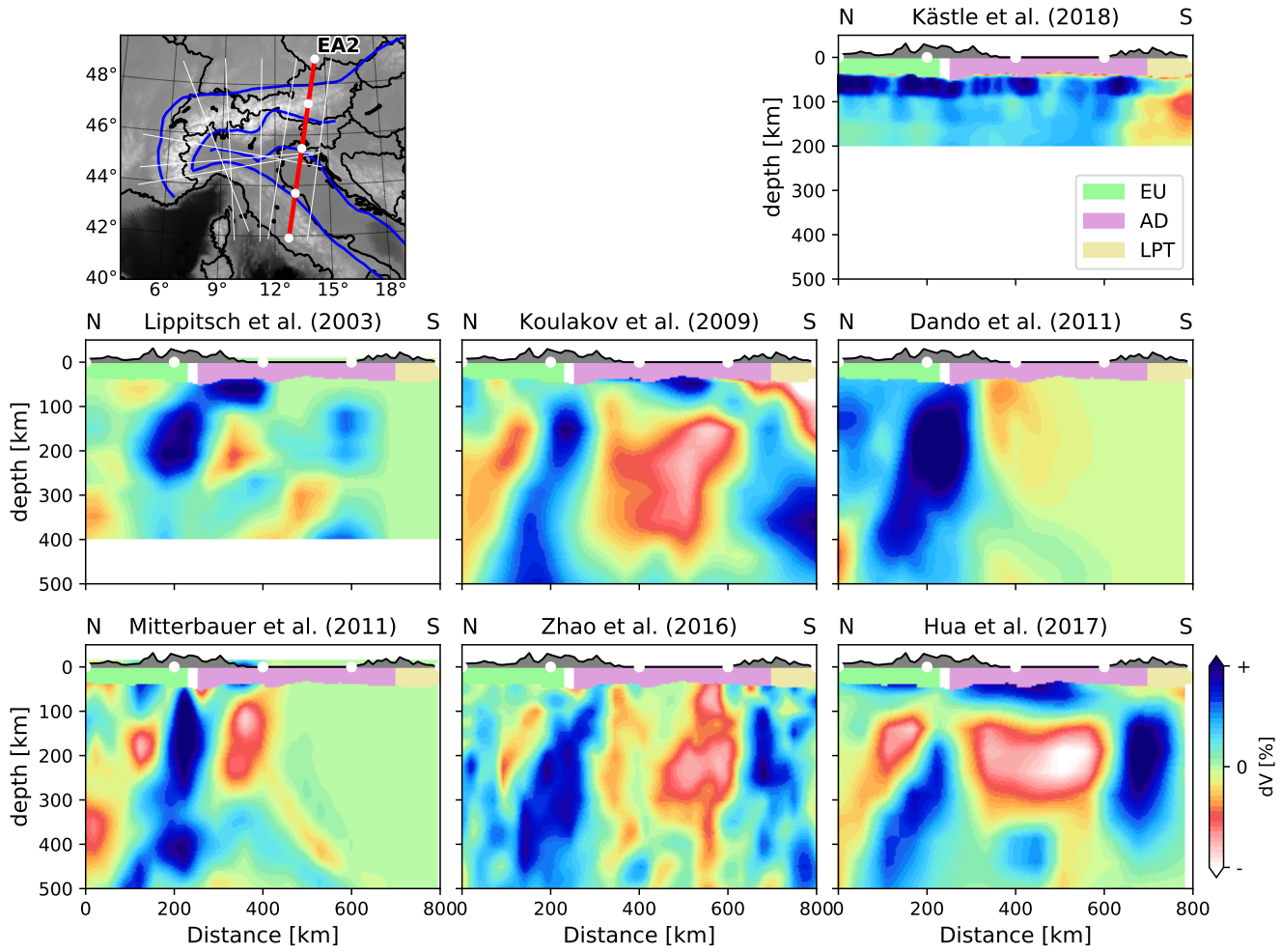


Figure S9. Cross-section comparison of different tomographic models. The colors show either shear-velocity deviations (Kästle et al., 2018) or compressional-velocity deviations (other models) of PREM (Dziewonski and Anderson, 1981). The color scale is normalized to $\pm 5\%$ for Lippitsch et al. (2003), $\pm 3.5\%$ for Kästle et al. (2018), $\pm 3\%$ for Koulakov et al. (2009); Zhao et al. (2016) and $\pm 2\%$ for the other models. Moho boundaries from Spada et al. (2013). EU: Europe, AD: Adria, LPT: Liguro-Provençal and Tyrrhenian basins. Faults and tectonic limits (blue lines in the map) simplified from Schmid et al. (2004, 2008); Handy et al. (2010).

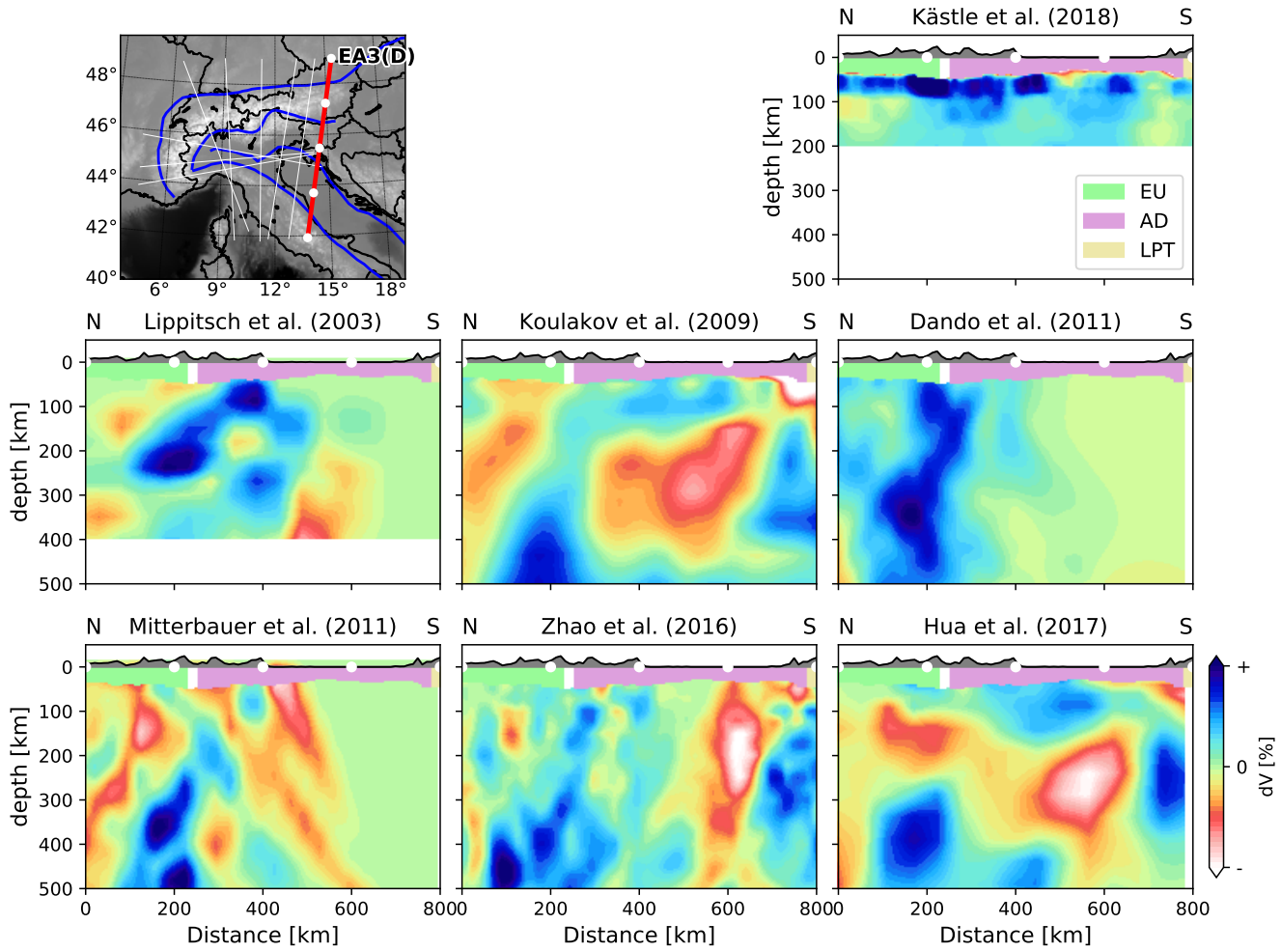


Figure S10. Cross-section comparison of different tomographic models. The colors show either shear-velocity deviations (Kästle et al., 2018) or compressional-velocity deviations (other models) of PREM (Dziewonski and Anderson, 1981). The color scale is normalized to $\pm 5\%$ for Lippitsch et al. (2003), $\pm 3.5\%$ for Kästle et al. (2018), $\pm 3\%$ for Koulakov et al. (2009); Zhao et al. (2016) and $\pm 2\%$ for the other models. Moho boundaries from Spada et al. (2013). EU: Europe, AD: Adria, LPT: Liguro-Provençal and Tyrrhenian basins. Faults and tectonic limits (blue lines in the map) simplified from Schmid et al. (2004, 2008); Handy et al. (2010).

References

- Brückl, E.: Lithospheric structure and tectonics of the eastern Alps-evidence from new seismic data, INTECH Open Access Publisher, 2011.
- Dando, B., Stuart, G., Houseman, G., Hegedüs, E., Brückl, E., and Radovanović, S.: Teleseismic tomography of the mantle in the Carpathian-Pannonian region of central Europe, *Geophysical Journal International*, 186, 11–31, 2011.
- Dziewonski, A. M. and Anderson, D. L.: Preliminary reference Earth model, *Physics of the earth and planetary interiors*, 25, 297–356, 1981.
- Handy, M. R., Schmid, S. M., Bousquet, R., Kissling, E., and Bernoulli, D.: Reconciling plate-tectonic reconstructions of Alpine Tethys with the geological-geophysical record of spreading and subduction in the Alps, *Earth-Science Reviews*, 102, 121–158, 2010.
- Hetényi, G., Plomerová, J., Bianchi, I., Exnerová, H. K., Bokelmann, G., Handy, M. R., Babuška, V., Group, A.-E. W., et al.: From mountain summits to roots: Crustal structure of the Eastern Alps and Bohemian Massif along longitude 13.3° E, *Tectonophysics*, 744, 239–255, 2018.
- Hua, Y., Zhao, D., and Xu, Y.: P-wave anisotropic tomography of the Alps, *Journal of Geophysical Research: Solid Earth*, 2017.
- Kästle, E. D., El-Sharkawy, A., Boschi, L., Meier, T., Rosenberg, C., Bellahsen, N., Cristiano, L., and Weidle, C.: Surface Wave Tomography of the Alps Using Ambient-Noise and Earthquake Phase Velocity Measurements, *Journal of Geophysical Research: Solid Earth*, 123, 1770–1792, 2018.
- Koulakov, I., Kaban, M., Tesauro, M., and Cloetingh, S.: P-and S-velocity anomalies in the upper mantle beneath Europe from tomographic inversion of ISC data, *Geophysical Journal International*, 179, 345–366, 2009.
- Kummerow, J., Kind, R., Oncken, O., Giese, P., Ryberg, T., Wylegalla, K., Scherbaum, F., Group, T. W., et al.: A natural and controlled source seismic profile through the Eastern Alps: TRANSALP, *Earth and Planetary Science Letters*, 225, 115–129, 2004.
- Lippitsch, R., Kissling, E., and Ansorge, J.: Upper mantle structure beneath the Alpine orogen from high-resolution teleseismic tomography, *Journal of Geophysical Research: Solid Earth*, 108, 2003.
- Mitterbauer, U., Behm, M., Brückl, E., Lippitsch, R., Guterch, A., Keller, G. R., Koslovskaya, E., Rumpfhuber, E.-M., and Šumanovac, F.: Shape and origin of the East-Alpine slab constrained by the ALPASS teleseismic model, *Tectonophysics*, 510, 195–206, 2011.
- Nussbaum, C.: Neogene tectonics and thermal maturity of sediments of the easternmost southern Alps (Friuli area, Italy), PhD thesis, 2000.
- Schmid, S. M., Fügenschuh, B., Kissling, E., and Schuster, R.: Tectonic map and overall architecture of the Alpine orogen, *Eclogae Geologicae Helvetiae*, 97, 93–117, 2004.
- Schmid, S. M., Bernoulli, D., Fügenschuh, B., Matenco, L., Schefer, S., Schuster, R., Tischler, M., and Ustaszewski, K.: The Alpine-Carpathian-Dinaridic orogenic system: correlation and evolution of tectonic units, *Swiss Journal of Geosciences*, 101, 139–183, 2008.
- Schönborn, G.: Balancing cross sections with kinematic constraints: the Dolomites (northern Italy), *Tectonics*, 18, 527–545, 1999.
- Spada, M., Bianchi, I., Kissling, E., Agostinetti, N. P., and Wiemer, S.: Combining controlled-source seismology and receiver function information to derive 3-D Moho topography for Italy, *Geophysical Journal International*, 194, 1050–1068, 2013.
- Ustaszewski, K., Schmid, S. M., Fügenschuh, B., Tischler, M., Kissling, E., and Spakman, W.: A map-view restoration of the Alpine-Carpathian-Dinaridic system for the Early Miocene, in: *Orogenic Processes in the Alpine Collision Zone*, pp. S273–S294, Springer, 2008.
- Zhao, L., Paul, A., Malusà, M. G., Xu, X., Zheng, T., Solarino, S., Guillot, S., Schwartz, S., Dumont, T., Salimbeni, S., et al.: Continuity of the Alpine slab unraveled by high-resolution P wave tomography, *Journal of Geophysical Research: Solid Earth*, 2016.